ACS APPLIED MATERIALS & INTERFACES

Article

Label-free electrochemical sensing platform for microRNA-21 detection using thionine and gold nanoparticles co-functionalized MoS2 nanosheet

Dan Zhu, Wei Liu, Dongxia Zhao, Qing Hao, Jing Li, Jiaxuan Huang, Jiye Shi, Jie Chao, Shao Su, and Lianhui Wang

ACS Appl. Mater. Interfaces, **Just Accepted Manuscript** • DOI: 10.1021/acsami.7b11385 • Publication Date (Web): 26 Sep 2017

Just Accepted

ACS Publications

ACS Applied Materials & Interfaces is published by the American Chemical Society.
1155 Sixteenth Street N.W., Washington, DC 20036

Label-Free Electrochemical Sensing Platform for MicroRNA-21 Detection Using Thionine and Gold Nanoparticles Co-Functionalized MoS_2 Nanosheet

Dan Zhu[†, ǁ], Wei Liu[†, ǁ], Dongxia Zhao[†], Qing Hao[†], Jing Li[†], Jiaxuan Huang[†], Jiye Shi[‡], Jie Chao[†], Shao Su[*, †], Lianhui Wang[*, †]

[†]Key Laboratory for Organic Electronics & Information Displays (KLOEID), Institute of Advanced Materials (IAM), National Syngerstic Innovation Center for Advanced Materials (SICAM), Nanjing University of Posts &Telecommunications, 9 Wenyuan Road, Nanjing 210023, China

[‡]UCB Pharma, 208 Bath Road, Slough, SL1 3WE, United Kingdom

ABSTRACT

Herein, we demonstrated a label-free and simple electrochemical sensing platform to detect microRNA-21 (miR-21) with highly sensitivity by using MoS_2 nanosheet functionalized with thionine and gold nanoparticles (MoS_2-Thi-AuNPs). Interestingly, thionine (Thi) was used as reducing agent to successfully synthesize MoS_2-Thi-AuNPs nanohybrid and as a signaling molecule to monitor DNA-RNA hybridization, which provided an ideal platform for label-free miR-21 detection. Upon hybridization with miR-21, the formation of DNA-RNA duplex on the electrode would greatly hinder the electron transfer, which caused the electrochemical signal decrease of Thi. After experimental condition optimization, the signal change of peak currents of Thi have a linear relation with the logarithm of miR-21 concentration ranging from 1.0 pM to 10.0 nM and the limit of detection (LOD) was 0.26 pM. Moreover, such biosensor could detect miR-21 in biological samples like human serum with satisfactory results.

KEYWORDS: molybdenum disulfide (MoS_2), gold nanoparticles (AuNPs), thionine (Thi), electrochemical biosensor, microRNA

INTRODUCTION

MicroRNA (miRNA) is a class of non-coding single-stranded RNA molecule with a length of 18-25 nucleotides, which has important regulation effect in diverse biological processes in organisms. Recent studies have demonstrated that miRNA participates in the cell growth, tissue differentiation and other disease state process.[1, 2] Abnormal expression of miRNA may relate to the existence of cancer disease and even small expression level changes of miRNA could influence to the expression of genes significantly. For example, circulating miRNAs exist in the peripheral blood, which have a close relationship with specific cancer and have been considered as reliable biomarkers for cancer therapy.[3, 4] In many cancerous tissues like breast cancer, lung adenocarcinomas and hepatocellular carcinoma, the expression level of miRNA-21 (miR-21) is significantly increased.[5-7] Therefore, the determination of concentration of miRNA in biological samples has profound importance in pathological and diagnosis studies. However, the simple, precise and low-cost quantification of miRNA is always challenging. The most common methods for miRNA quantification are real-time fluorescent quantitative polymerase chain reaction (RT-PCR),[8] northern blotting[9] and microarrays,[10] which are found to be time-consuming and less sensitive.

In recent years, electrochemical sensor is emerging as a powerful tool for biosensing and has attracted great interest on account of its high sensitivity, specificity and inexpensive equipment.[11, 12] By integrating with unique features and functions of nanomaterials, various electrochemical sensors for miRNAs detection are developed to enhance the electron transferring, improve capture efficient and amplify the sensing signals, such as noble nanoparticles, graphene oxide, DNA nanostructures and nanodiamonds.[13-17] For example, Rahaie developed an ultrasensitive electrochemical sensor to detect miR-155 by using graphene oxide and gold nanorod with an intercalating label Oracet Blue as signal indicator.[18] Ma developed a sensitive electrochemical biosensor for miRNA detection with horseradish peroxidase (HRP) functionalized graphene quantum dot as sensing element.[19] Xie employed carbon nanotubes, DNA nanostructures and nanodiamonds to immobilize DNA probes and

hybridization chain reaction (HCR) functionalized DNAzyme nanowires as signal indicator.[17] However, most of the works adopted two or more steps to capture target miRNA and introduced signal indicator, which could complicate the detection procedure during the process. Therefore, label-free biosensors have attracted wide attention because it simplified the assembling processes and provided an effective way for target sensing. Some researchers employed electrochemical impedance spectroscopy (EIS) measurements[21,22] to directly monitor the surface of the electrode. However, EIS results were always easily disturbed by surface contamination and adsorption. Therefore, it is significant to develop a simple, efficient and label-free platform to detect miRNA by using electrochemical indicator-functionalized nanomaterials with high sensitivity and selectivity.

Molybdenum disulfide (MoS_2) is a new two-dimensional lamellar nanomaterials with graphene-like lamellar structure, novel physical photoelectric and chemical properties. In recent years, MoS_2 has become an ideal base material due to its excellent performance in easy modification and super-large specific surface area, which could react with abundant nanomaterials (like noble metals, metal oxides) and organic molecules to form novel nanocomposite. Various biosensor platforms based on MoS_2 were built to achieve highly sensitive detection for biological or chemical molecules. For instance, Zhang's group reported the first example of the target-induced displacement assay for DNA and small molecules detection in solution based on the fluorescence quenching capacity of MoS_2 nanosheet.[22] Lin and Li's group developed the electrochemical biosensor for the direct detection of H_2O_2 by taking the advantage of the inherent electrocatalytical activity of thin-layer MoS_2.[23] Yang and Jiao's group reported an electrochemical assay for direct detection of DNA based on the adsorption between single-strand/double-strand DNA and thin-layer MoS_2 nanosheets. An ultrahigh sensitivity could be achieved by taking the advantage of large surface area of MoS_2.[24] To further expand the properties of MoS_2, our group have developed a series of electrochemical biosensors based on metal-decorated MoS_2 for the detection of various biomolecules, like protein, dopamine, adenosine triphosphate and thrombin with high sensitivity and selectivity.[25-29]

Herein, we demonstrated a simple and rapid hybridization assay for label-free miR-21 detection based on our rationally designed MoS_2 nanosheet modified with thionine and gold nanoparticles (MoS_2-Thi-AuNPs). DNA worked as recognition probes and thionine (Thi) was employed as an electrochemical indicator for subsequent electrochemical detection and reducing agent for the reduction of $HAuCl_4$. The MoS_2-Thi-AuNPs nanocomposite were synthesized by microwave-assisted hydrothermal method[29] and then assembled onto the glassy carbon electrode (GCE) by adsorption (Figure 1). After that, capture DNA was assembled on the nanosheet to form recognition layer. Due to the electron transfer between Thi and the electrode, the current peaks of Thi could be obviously observed. After the hybridization with miR-21, duplex DNA-RNA structure was formed, which would greatly hinder the electron transfer on the electrode and caused the signal decrease of Thi. The highly sensitive detection of miR-21 with high specificity was achieved by measuring the decreasement of Thi electrochemical signal. The detection limit was calculated to be 0.26 pM (S/N = 3). More importantly, the binding of Au-S was robust and the target hybridization-induced signal change allowed the detection of specific target in the real samples.

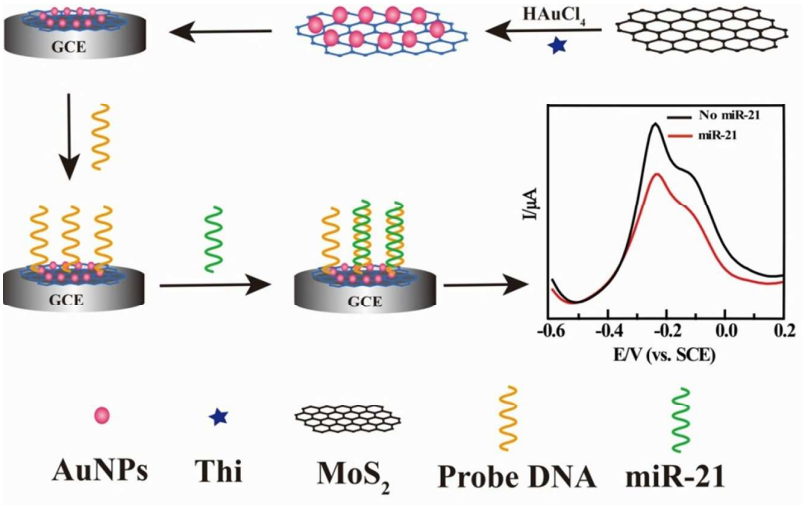

Figure 1. Schematic fabrication of electrochemical platform for miR-21 detection based on MoS_2 nanosheet modified with thionine and gold nanoparticles (MoS_2-Thi-AuNPs).

MATERIALS AND METHODS

Chemicals and Apparatus.

The details information was provided in Supporting Information.

Preparation of MoS_2 nanosheet and MoS_2-Thi-AuNPs nanocomposite.

MoS_2 nanosheet and MoS_2-Thi-AuNPs nanocomposite were synthesized according to our previous works.[29,30] The details were demonstrated in Supporting Information.

Fabrication of the MoS_2-based electrochemical biosensor.

A glassy carbon electrode (GCE) (3 mm in diameter) was treated with alumina powder, water, ethanol in succession. After being dried under nitrogen, MoS_2-Thi-AuNPs nanocomposite was modified on the electrode, which was defined as MoS_2-Thi-AuNPs/GCE. After that, 1 μM probe DNA was dropped onto the electrode's surface and incubated at 25 ^{o}C for 16 h. The unbounded probe DNA was removed from the modified electrode by rinsing 3 times with 10 mM Tris-HCl (pH 7.4). Then, 1 mM MCH was incubated for 60 min in the reaction buffer at 37 °C to block the active surface of electrode. Finally, the as-prepared electrode based on MoS_2-Thi-AuNPs was used to detect target miR-21 with various concentrations under optimal condition.

The detection of miR-21.

The miR-21 solution with different concentrations was firstly diluted by 10 mM Tris-HCl with 140 mM NaCl and 5 mM $MgCl_2$ (pH=7.4). Then, 5 μL miRNA solution was added to the surface of MoS_2-Thi-AuNPs modified electrode. After 50 minutes hybridization, unreacted miR-21 was removed by using 10 mM Tris-HCl (pH 7.4) for 3 times. The electrochemical detection was performed in 10 mM Tris-HCl (pH 7.4). For SWV measurement, the detection time was 8 s and the scanning rate was 0.1 V/s and the range was -0.6 V to 0.2 V.

RESULTS AND DISCUSSION

Characterization of MoS_2 nanosheet and MoS_2-Thi-AuNPs nanocomposite.

From the transmission electron microscopy (TEM) image (Figure 2A), a typical wrinkled and thin-layered nanostructure was observed, indicating that few layers

MoS_2 nanosheet was exfoliated successfully. After being reacted with $HAuCl_4$ and Thi, 40 nm well-dispersed clover-shape AuNPs were formed on the surface of MoS_2 nanosheet (Figure 2B), suggesting that MoS_2-Thi-AuNPs nanocomposite had been successfully synthesized. The size statistical analysis indicated that AuNPs' diameter was normal distributed with ~40 nm in average (Figure S1). Furthermore, we employed UV-vis spectrum to record the process of reaction and the result was shown in Figure S2A. Two board peaks located ranging from 240 to 290 nm and from 530 to 650 nm of MoS_2-Thi-AuNPs were observed in the spectra, which were corresponding to the peaks of MoS_2 nanosheet, Thi and gold nanoparticles. Meanwhile, the color solution of MoS_2-Thi-AuNPs nanocomposite presented to be light grayish green, which was different from that of MoS_2 nanosheet (light brown) and Thi (blue) solution (Figure S2B). The scanning electron microscope (SEM) image and energy dispersive spectrometer (EDS) results confirmed that the Mo, N, S and Au elements were existed in the nanocomposite, proving that AuNPs had successfully supported on the MoS_2 nanosheet (Figure S3). Furthermore, the data of X-Ray Diffraction (XRD, Figure S4) and X-ray photoelectron spectroscopy (XPS, Figure S5) also proved the existence of Thi and AuNPs on MoS_2 nanosheet's surface. All data showed that the MoS_2-Thi-AuNPs nanocomposite was successfully prepared.

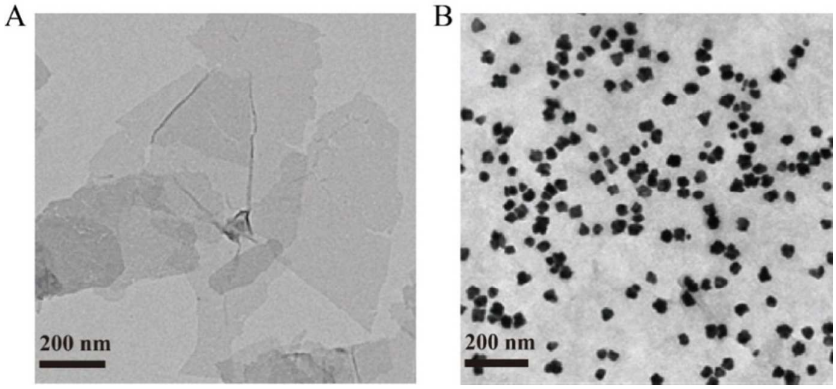

Figure 2. Transmission electron microscopy (TEM) imaging of (A) as-prepared MoS_2 nanosheets and (B) synthetic MoS_2-Thi-AuNPs nanocomposite.

Electrochemical characterization of MoS_2-Thi-AuNPs/GCE biosensor.

The modification steps of the MoS_2-based biosensor was characterized by electrochemical impedance spectroscopy (EIS) technique in 5 mM $[Fe(CN)_6]^{3-/4-}$ and

0.1 M KCl (Figure 3A). The electron-transfer resistance (R_{et}) of each modified electrodes was estimated from the scale of the semicircle. The result depicted that the R_{et} of bare GCE was only 78 Ω (curve a). If MoS_2-Thi-AuNPs was successfully immobilized onto the surface of GCE (curve b), the R_{et} was increased significantly to 192 Ω. After being functionalized with probe DNA, the R_{et} of the electrode was increased to 305 Ω (curve c) because DNA was negative charge. Then, the R_{et} was further increased to about 343 Ω (curve d) after MCH blocking the remaining active sites of the electrode's surface. A larger R_{et} (592 Ω) was then obtained after miR-21 be recognized by probe DNA (curve e), suggesting that the double-strand structure of DNA-RNA duplex hindered the electron transfer. The EIS results showed that the MoS_2-based platform was successfully constructed and the designed detection strategy was worked.

Thi is a commonly used electrochemical indicator, which is employed as signal indicator to test the detection feasibility in this work. Figure 3B demonstrated the square wave voltammetry (SWV) curves of different modified electrodes in 10 mM Tris-HCl (pH 7.4). For bare GCE, no obvious peak was observed (curve a in Figure 3B). After being modified with MoS_2-Thi-AuNPs nanocomposite, a distinct anodic peak current of Thi at -0.23 V was observed (curve b in Figure 3B), indicating that Thi in the nanocomposite still had good electrochemical activity. After being functionalized by probe DNA, the current value of Thi was greatly decreased (curve c in Figure 3B) because the assembled DNA hindered the electron transfer on the electrode. Then the current was continue to decline after MCH blocking (curve d in Figure 3B) and miR-21 hybridization (curve e in Figure 3B), respectively. This phenomenon was corresponding with the results of EIS test, which further proved that the designed sensing platform had a good performance in target recognition and signal indicating.

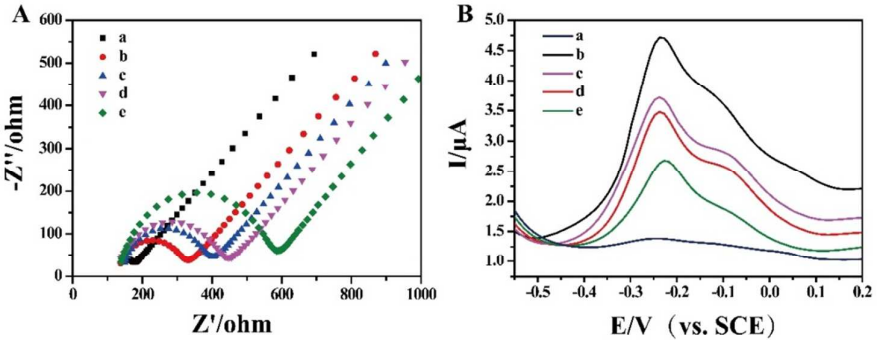

Figure 3. (A) Nyquist plots and (B) SWV curves of (a) bare GCE, (b) MoS_2-Thi-AuNPs/GCE, (c) DNA/MoS_2-Thi-AuNPs/GCE, (d) MCH/DNA/MoS_2-Thi-AuNPs/GCE, and (e) miR-21/MCH/DNA/MoS_2-Thi-AuNPs/GCE in 5 mM $K_3Fe(CN)_6$/ $K_4Fe(CN)_6$ (1:1) solution containing 0.1 M KCl and 10 mM Tris-HCl (pH 7.4), respectively. The concentration of probe DNA and miR-21 was 100 nM and 10 nM, respectively.

Condition optimization for detection.

To obtain the optimal reaction condition, the concentration of the probe DNA, the incubation time of probe DNA and the hybridization time between probe DNA and miR-21 were tested because these factors would directly affect the hybridization efficiency of the biosensor. The peak current decrement of Thi was defined as $\Delta I = I_{\text{no miR-21}} - I_{\text{miR-21}}$, while $I_{\text{no miR-21}}$ was the peak current at -0.23 V without miR-21 and $I_{\text{miR-21}}$ was the peak current with target miR-21. The probe concentration from 0.1 nM to 10 μM was tested and 1 μM was optimized as the loading concentration of probe DNA (Figure S6). Obviously, a maximum difference of peak current was observed when the incubation time was 16 h and did not change obviously after 16 h (Figure 4A). Therefore, we chose 16 h as the optimal incubation time for the detection of miR-21. Similarly, 50 min was selected as the hybridization time between probe DNA and miR-21. (Figure 4B).

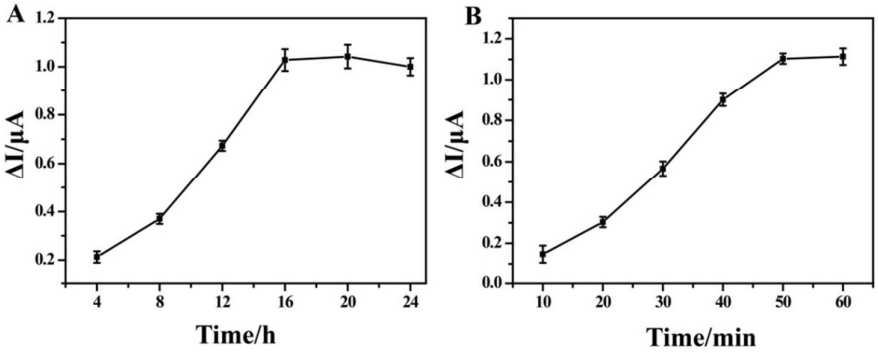

Figure 4. (A) The optimization for the incubation time of probe DNA from 4 to 24 h (4 h, 8 h, 12 h, 16 h, 20 h and 24 h) and (B) The optimization for the hybridization time between probe DNA and miR-21 from 10 to 60 min (10 min, 20 min, 30 min, 40 min, 50 min and 60 min).

Analytical performance of MoS_2-based biosensor.

Under the optimal conditions, SWV detection was adopted to investigate the detection performance of the MoS_2-based biosensor (Figure 5). Once the addition of miR-21, the current of Thi at -0.23 V was decreased (Figure 5A) and the dynamic range for miR-21 detection was checked. The peak currents variation of the biosensor kept a linear relation with the logarithm of the concentration of miR-21 from 1.0 pM-10 nM (Figure 5B). The obtained equation was ΔI (μA) = 0.204 $\log c_{miR\text{-}21}$ (pM) + 0.279 (R^2=0.996) and the LOD was calculated to be 0.26 pM (S/N=3). The detection performance was better than or comparable to some previous works,[31-36] which was listed in Table S2. The high sensitivity may attribute to the large surface area of MoS_2-Thi-AuNPs nanocomposites,[29] which allows the loading of large amounts of probe DNA for target miR-21 capturing and Thi for electrochemical sensing. Moreover, the AuNPs supported on MoS_2 was not only convenient for the immobilization of probe DNA through Au-S bond, but also increase the electronic conductivity of electrode,[37, 38] which is beneficial to increase the sensitivity of biosensor. The experimental data suggested that the MoS_2-Thi-AuNPs nanocomposite might be a potential candidate to construct electrochemical platform for target molecules detection.

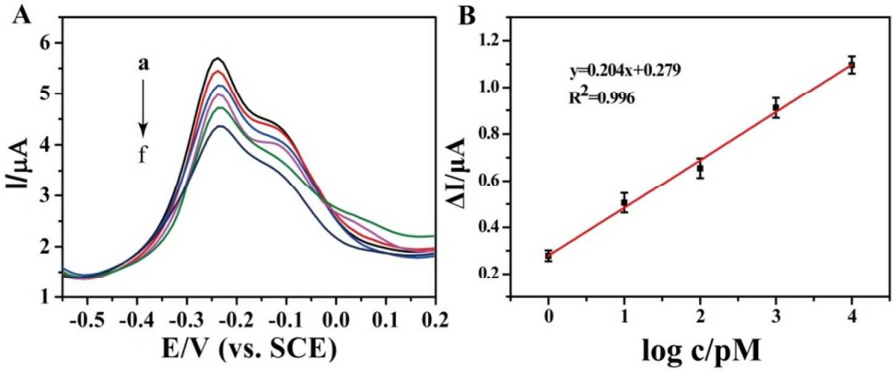

Figure 5. (A) SWV curves of the biosensor responded to various miR-21 concentrations (a-f: 0, 1.0, 10, 100, 1000 and 10000 pM). (B) Regression curves for miR-21 detection.

Selectivity test.

For the selectivity test, single-base terminal mismatched miRNA (SM-T), single-base middle mismatched miRNA (SM-M) and non-complementary miRNA (NC) were analyzed under the same condition. The SWV curves was recorded in Figure 6A. The calculated ΔI of the MoS_2-based biosensor for target miRNA detection was 1.9 times, 2.6 times and 20.0 times than that for SM-T, SM-M, NC, respectively (Figure 6B). It should be noted that the as-prepared MoS_2-based biosensor could effectively discriminate single-base terminal mismatched from single-base middle mismatch miRNA sequence. The result suggests that the mismatch site on terminal or in middle of the miRNA strand have a strong impact on the electrochemical signals. The reason may be that the DNA-RNA hybridization occurs to a lower extent for middle-mismatched sequence than that for terminal-mismatched sequence.[39, 40] All data indicated that the biosensor possessed excellent selectivity and discriminated ability.

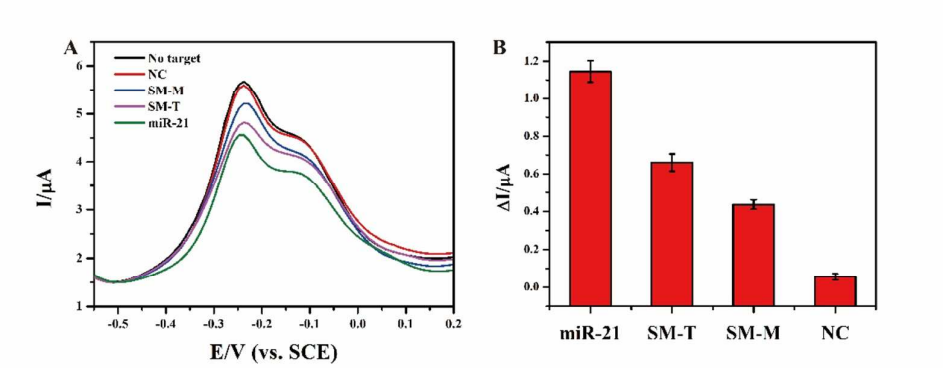

Figure 6. (A) Typical SWV curves of the MoS_2-based biosensor for the same concentration (10 nM) of target miR-21, single-base terminal mismatched miRNA (SM-T), single-base middle mismatched miRNA (SM-M) and non-complementary miRNA (NC) detection. (B) ΔI responses for miR-21 detection.

Real samples analysis.

To test the target miR-21 detection in biological samples, method of standard addition was adopted to analyze miR-21 in human serum. Various amounts of miR-21 (1 pM, 10 pM and 1000 pM) were spiked into 1% human serum. Each sample was then analyzed with the biosensors. As shown in Table 1, the relative standard deviation (RSD) of this biosensor was less than 7% and the recovery was more than 96%, indicating that the MoS_2-based biosensor had a potential application in real biological samples.

Table 1. Analysis data of the MoS_2-based sensor for miR-21 determination in human serum.

Sample	Added (pM)	Found (pM)	RSD (%)	Recovery (%)
1	1	1.03, 0.94, 1.07	6.57	101.0
2	10	9.26, 9.86, 9.74	3.30	96.2
3	1000	987.79, 1026.32, 976.56	2.61	99.6

CONCLUSIONS

In conclusion, we successfully fabricated a simple and efficient electrochemical platform for label-free detection of miR-21 based on a MoS_2-Thi-AuNPs nanocomposite, in which Thi was used as reducing agent for the reduction of $HAuCl_4$

and electrochemical signal indicator for miR-21 detection. It does not require the labeling of DNA or RNA strands and the whole detection time was within 1 h. Under optimal conditions, the biosensor had a wide linear range from 1.0 pM to 10 nM) and a low detection limit (0.26 pM). Moreover, the biosensor could effectively distinguish single-base mismatched miRNA from target miR-21. As expectedly, such MoS_2-based platform could determine miR-21 in real sample with satisfactory results, suggesting the MoS_2-based biosensor offered potential application in cancer-related biomolecules analysis.

ASSOCIATED CONTENT

Supporting Information

The Supporting Information is available free of charge via the Internet at http://pubs.acs.org.

The synthesis process of MoS_2 nanosheet and MoS_2-Thi-AuNPs nanocomposite, UV-vis absorption spectra and photo images of MoS_2 nanosheet, Thi and MoS_2-Thi-AuNPs nanocomposite, and the comparison of different nanomaterials-based electrochemical sensors for miRNA detection were listed in Supporting Information.

AUTHOR INFORMATION

Corresponding Author

* Email: iamssu@njupt.edu.cn, iamlhwang@njupt.edu.cn. Tel: +86 25 85866333.

[I]These authors contributed equally to this work.

Notes

The authors declare no competing financial interest.

ACKNOWLEDGEMENTS

This work was financially supported by the Key Research Program of National Nanotechnology and Science (2017YFA0205302) the National Natural Science Foundation of China (21475064, 21605087, 21373260 and 21305070), the Program for Changjiang Scholars and Innovative Research Team in University (IRT_15R37),

the Priority Academic Program Development of Jiangsu Higher Education Institutions (PAPD, YX03002), the China Postdoctoral Science Foundation funded project (BX201700123), the Scientific Research Foundation of Nanjing University of Posts and Telecommunications (NY215058), and the Natural Science Fund for Colleges and Universities in Jiangsu Province (16KJB150032).

REFERENCES

(1). Wienholds, E.; Kloosterman, W. P.; Miska, E.; Alvarez-Saavedra, E.; Berezikov, E.; de Bruijn, E.; Horvitz, H. R.; Kauppinen, S.; Plasterk, R. H. A. MicroRNA Expression in Zebrafish Embryonic Development. *Science.* **2005,** *309*, 310-311.

(2). Croce, C. M. Causes and Consequences of MicroRNA Dysregulation in Cancer. *Nat Rev Genet.* **2009,** *10*, 704-714.

(3). Iorio, M. V.; Croce, C. M. MicroRNA Dysregulation in Cancer: Diagnostics, Monitoring and Therapeutics. A Comprehensive Review. *Embo Molecular Medicine.* **2012,** *4*, 143-159.

(4). Bryant, R. J.; Pawlowski, T.; Catto, J. W. F.; Marsden, G.; Vessella, R. L.; Rhees, B.; Kuslich, C.; Visakorpi, T.; Hamdy, F. C. Changes in Circulating MicroRNA Levels Associated with Prostate Cancer. *Br. J. Cancer.* **2012,** *106*, 768-774.

(5). Yan, L. X.; Huang, X. F.; Shao, Q.; Huang, M. Y.; Deng, L.; Wu, Q. L.; Zeng, Y. X.; Shao, J. Y. MicroRNA MiR-21 Overexpression in Human Breast Cancer is Associated with Advanced Clinical Stage, Lymph Node Metastasis and Patient Poor Prognosis. *RNA.* **2008,** *14*, 2348-2360.

(6). Zhang, J. G.; Wang, J. J.; Zhao, F.; Liu, Q.; Jiang, K.; Yang, G. H. MicroRNA-21 (MiR-21) Represses Tumor Suppressor PTEN and Promotes Growth and Invasion in Non-small Cell Lung Cancer (NSCLC). *Clin Chim Acta.* **2010,** *411*, 846-852.

(7). Najafi, Z.; Sharifi, M.; Javadi, G. Degradation of MiR-21 Induces Apoptosis and Inhibits Cell Proliferation in Human Hepatocellular Carcinoma. *Cancer Gene Ther.* **2015,** *22*, 530-535.

(8). Redshaw, N.; Wilkes, T.; Whale, A.; Cowen, S.; Huggett, J.; Foy, C. A. A Comparison of MiRNA Isolation and RT-qPCR Technologies and Their Effects

on Quantification Accuracy and Repeatability. *Biotechniques.* **2013,** *54*, 155-164.

(9). Pall, G. S.; Codony-Servat, C.; Byrne, J.; Ritchie, L.; Hamilton, A. Carbodiimide-mediated Cross-Linking of RNA to Nylon Membranes Improves the Detection of SiRNA, MiRNA and PiRNA by Northern Blot. *Nucleic Acids Res.* **2007,** *35*, e60.

(10). Zhao, J. J.; Yang, J.; Lin, J.; Yao, N.; Zhu, Y.; Zheng, J.; Xu, J.; Cheng, J. Q.; Lin, J. Y.; Ma, X. Identification of MiRNAs Associated with Tumorigenesis of Retinoblastoma by MiRNA Microarray Analysis. *Child's Nerv Syst.* **2009,** *25*, 13-20.

(11). Kimmel, D. W.; LeBlanc, G.; Meschievitz, M. E.; Cliffel, D. E., Electrochemical Sensors and Biosensors. *Anal. Chem.* **2012,** *84*, 685-707.

(12). Yang, F.; Zuo, X.; Li, Z.; Deng, W.; Shi, J.; Zhang, G.; Huang, Q.; Song, S.; Fan, C., A Bubble-Mediated Intelligent Microscale Electrochemical Device for Single-step Quantitative Bioassays. *Adv. Mater.* **2014,** *26*, 4671-4676.

(13). Su, S.; Wu, Y.; Zhu, D.; Chao, J.; Liu, X.; Wan, Y.; Su, Y.; Zuo, X.; Fan, C.; Wang, L. On-Electrode Synthesis of Shape-Controlled Hierarchical Flower-like Gold Nanostructures for Efficient Interfacial DNA Assembly and Sensitive Electrochemical Sensing of MicroRNA. *Small.* **2016,** *12*, 3794-3801.

(14). Lin, M.; Wen, Y.; Li, L.; Pei, H.; Liu, G.; Song, H.; Zuo, X.; Fan, C.; Huang, Q. Target-responsive, DNA Nanostructure-Based E-DNA Sensor for MicroRNA Analysis. *Anal. Chem.* **2014,** *86*, 2285-2288.

(15). Ge, Z.; Pei, H.; Wang, L.; Song, S.; Fan, C., Electrochemical Single Nucleotide Polymorphisms Genotyping on Surface Immobilized Three-Dimensional Branched DNA Nanostructure. *Sci. China-Chem.* **2011,** *54*, 1273-1276.

(16). Ye, D.; Zuo, X.; Fan, C., DNA Nanostructure-Based Engineering of the Biosensing Interface for Biomolecular Detection. *Prog. Chem.* **2017,** *29*, 36-46.

(17). Liu, L.; Song, C.; Zhang, Z.; Yang, J.; Zhou, L.; Zhang, X.; Xie, G. Ultrasensitive Electrochemical Detection of MicroRNA-21 Combining Layered Nanostructure of Oxidized Single-Walled Carbon Nanotubes and Nanodiamonds

by Hybridization Chain Reaction. *Biosens. Bioelectron.* **2015,** *70*, 351-357.

(18). Azimzadeh, M.; Rahaie, M.; Nasirizadeh, N.; Ashtari, K.; Naderi-Manesh, H. An Electrochemical Nanobiosensor for Plasma MiRNA-155, Based on Graphene Oxide and Gold Nanorod, for Early Detection of Breast Cancer. *Biosens. Bioelectron.* **2016,** *77*, 99-106.

(19). Hu, T.; Zhang, L.; Wen, W.; Zhang, X.; Wang, S. Enzyme Catalytic Amplification of MiRNA-155 Detection with Graphene Quantum Dot-Based Electrochemical Biosensor. *Biosens. Bioelectron.* **2016,** *77*, 451-456.

(20). Zhang, J.; Wu, D.-Z.; Cai, S.-X.; Chen, M.; Xia, Y.-K.; Wu, F.; Chen, J.-H. An Immobilization-free Electrochemical Impedance Biosensor Based on Duplex-specific Nuclease Assisted Target Recycling for Amplified Detection of MicroRNA. *Biosens. Bioelectron.* **2016,** *75*, 452-457.

(21). Capaldo, P.; Alfarano, S. R.; Ianeselli, L.; Dal Zilio, S.; Bosco, A.; Parisse, P.; Casalis, L. Circulating Disease Biomarker Detection in Complex Matrices: Real-Time, in Situ Measurements of DNA/miRNA Hybridization via Electrochemical Impedance Spectroscopy. *ACS Sens.* **2016,** *1*, 1003-1010.

(22). Zhu, C.; Zeng, Z.; Li, H.; Li, F.; Fan, C.; Zhang, H. Single-Layer MoS_2-Based Nanoprobes for Homogeneous Detection of Biomolecules. *J. Am. Chem. Soc.* **2013,** *135*, 5998-6001.

(23). Wang, T.; Zhu, H.; Zhuo, J.; Zhu, Z.; Papakonstantinou, P.; Lubarsky, G.; Lin, J.; Li, M. Biosensor Based on Ultrasmall MoS_2 Nanoparticles for Electrochemical Detection of H_2O_2 Released by Cells at the Nanomolar Level. *Anal. Chem.* **2013**, *85*, 10289-10295.

(24). Wang, X.; Nan, F.; Zhao, J.; Yang, T.; Ge, T.; Jiao, K. A Label-Free Ultrasensitive Electrochemical DNA Sensor Based on Thin-layer MoS_2 Nanosheets with High Electrochemical Activity. *Biosens. Bioelectron.* **2015,** *64*, 386-391.

(25). Su, S.; Fan, J.; Xue, B.; Yuwen, L.; Liu, X.; Pan, D.; Fan, C.; Wang, L. DNA-Conjugated Quantum Dot Nanoprobe for High-Sensitivity Fluorescent Detection of DNA and Micro-RNA. *ACS Appl. Mater. Interfaces.* **2014,** *6*,

1152-1157.

(26). Su, S.; Sun, H.; Xu, F.; Yuwen, L.; Wang, L. Highly Sensitive and Selective Determination of Dopamine in the Presence of Ascorbic Acid Using Gold Nanoparticles-Decorated MoS_2 Nanosheets Modified Electrode. *Electroanalysis.* **2013,** *25*, 2523-2529.

(27). Sun, H.; Chao, J.; Zuo, X.; Su, S.; Liu, X.; Yuwen, L.; Fan, C.; Wang, L. Gold Nanoparticle-Decorated MoS_2 Nanosheets for Simultaneous Detection of Ascorbic Acid, Dopamine and Uric Acid. *RSC Adv.* **2014,** *4*, 27625-27629.

(28). Su, S.; Sun, H.; Cao, W.; Chao, J.; Peng, H.; Zuo, X.; Yuwen, L.; Fan, C.; Wang, L. Dual-Target Electrochemical Biosensing Based on DNA Structural Switching on Gold Nanoparticle-Decorated MoS_2 Nanosheets. *ACS App. Mater. Interfaces.* **2016,** *8*, 6826-6833.

(29). Su, S.; Zou, M.; Zhao, H.; Yuan, C.; Xu, Y.; Zhang, C.; Wang, L.; Fan, C.; Wang, L. Shape-Controlled Gold Nanoparticles Supported on MoS_2 Nanosheets: Synergistic Effect of Thionine and MoS_2 and Their Application for Electrochemical Label-Free Immunosensing. *Nanoscale.* **2015,** *7*, 19129-19135.

(30). Yuwen, L.; Xu, F.; Xue, B.; Luo, Z.; Zhang, Q.; Bao, B.; Su, S.; Weng, L.; Huang, W.; Wang, L. General Synthesis of Noble Metal (Au, Ag, Pd, Pt) Nanocrystal Modified MoS_2 Nanosheets and the Enhanced Catalytic Activity of Pd-MoS_2 for Methanol Oxidation. *Nanoscale.* **2014,** *6*, 5762-5769.

(31). Kilic, T.; Topkaya, S. N.; Ariksoysal, D. O.; Ozsoz, M.; Ballar, P.; Erac, Y.; Gozen, O. Electrochemical Based Detection of MicroRNA, Mir21 in Breast Cancer Cells. *Biosens. Bioelectron.* **2012,** *38*, 195-201.

(32). Zhou, Y.; Wang, M.; Meng, X.; Yin, H.; Ai, S. Amplified Electrochemical MicroRNA Biosensor Using a Hemin-G-Quadruplex Complex as the Sensing Element. *RSC Adv.* **2012,** *2*, 7140-7145.

(33). Wu, X.; Chai, Y.; Yuan, R.; Su, H.; Han, J. A Novel Label-Free Electrochemical MicroRNA Biosensor Using Pd Nanoparticles as Enhancer and Linker. *Analyst.* **2013,** *138*, 1060-1066.

(34). Gao, Z.; Yu, Y. H. A MicroRNA Biosensor Based on Direct Chemical

Ligation and Electrochemically Amplified Detection. *Sens. Actuators B.* **2007,** *121*, 552-559.

(35). Zhou, Y.; Zhang, Z.; Xu, Z.; Yin, H.; Ai, S. MicroRNA-21 Detection Based on Molecular Switching by Amperometry. *New J. Chem.* **2012,** *36*, 1985-1991.

(36). Yin, H.; Zhou, Y.; Zhang, H.; Meng, X.; Ai, S. Electrochemical Determination of MicroRNA-21 Based on Graphene, LNA Integrated Molecular Beacon, AuNPs and Biotin Multifunctional Bio Bar Codes and Enzymatic Assay System. *Biosens. Bioelectron.* **2012,** *33*, 247-253.

(37). Su, S.; Sun, H.; Xu, F.; Yuwen, L.; Fan, C.; Wang, L. Direct Electrochemistry of Glucose Oxidase and a Biosensor for Glucose Based on a Glass Carbon Electrode Modified with MoS_2 Nanosheets Decorated with Gold Nanoparticles. *Microchim. Acta* **2014,** *181*, 1497-1503.

(38). Su, S.; Cao, W.; Liu, W.; Lu, Z.; Zhu, D.; Chao, J.; Weng, L.; Wang, L.; Fan, C.; Wang, L. Dual-mode Electrochemical Analysis of MicroRNA-21 Using Gold Nanoparticle-Decorated MoS_2 Nanosheet. *Biosens. Bioelectron.* **2017,** *94*, 552-559.

(39). Yang, S. Y.; Son, S.; Jang, S.; Kim, H.; Jeon, G.; Kim, W. J.; Kim, J. K. DNA-Functionalized Nanochannels for SNP Detection. Nano Lett. **2011,** *11,* 1032-1035.

(40). Garcia, T.; Revenga-Parra, M.; Abruna, H. D.; Pariente, F.; Lorenzo, E. Single-Mismatch Position-Sensitive Detection of DNA Based on a Bifunctional Ruthenium Complex. *Anal. Chem.* **2008,** *80*, 77-84.

TOC only

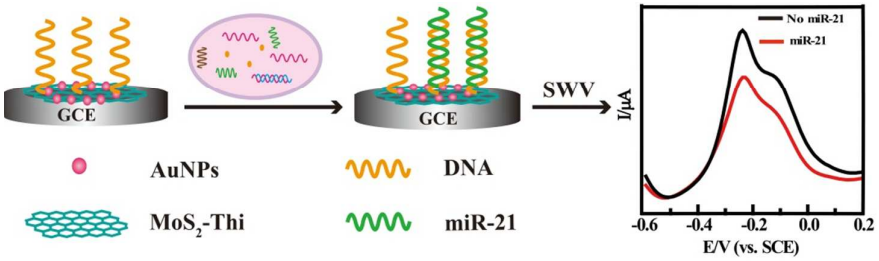
GCE
GCE
SWV
No miR-21
miR-21
I/μA
-0.6
-0.4
-0.2
0.0
0.2
E/V (vs. SCE)
AuNPs
DNA
MoS2-Thi
miR-21